AGU PUBLICATIONS

Geophysical Research Letters

RESEARCH LETTER
10.1002/2016GL072251

Key Points:
- With a 1-D PIC simulation model, multiband chorus has been successfully reproduced for the first time
- Our simulation results provide a theoretical support to the mechanism of lower band cascade to generate multiband chorus
- This nonlinear wave-wave coupling process shows a new pattern of evolution for whistler-mode waves in the Earth's magnetosphere

Correspondence to:
X. Gao, and Q. Lu,
qmlu@ustc.edu.cn

Citation:
Gao, X., Y. Ke, Q. Lu, L. Chen, and S. Wang (2017), Generation of Multiband Chorus in the Earth's Magnetosphere: 1-D PIC Simulation, *Geophys. Res. Lett.*, *44*, 618–624, doi:10.1002/2016GL072251.

Received 5 DEC 2016
Accepted 7 JAN 2017
Accepted article online 10 JAN 2017
Published online 21 JAN 2017

Generation of Multiband Chorus in the Earth's Magnetosphere: 1-D PIC Simulation

Xinliang Gao[1,2], Yangguang Ke[1,2], Quanming Lu[1,2], Lunjin Chen[3], and Shui Wang[1,2]

[1]CAS Key Laboratory of Geospace Environment, Department of Geophysics and Planetary Science, University of Science and Technology of China, Hefei, China, [2]Collaborative Innovation Center of Astronautical Science and Technology, Hefei, China, [3]Department of Physics, University of Texas at Dallas, Richardson, Texas, USA

Abstract Multiband chorus waves, where the frequency of upper band chorus is about twice that of lower band chorus, have recently been reported based on THEMIS observations. The generation of multiband chorus waves is attributed to the mechanism of lower band cascade, where upper band chorus is excited via the nonlinear coupling process between lower band chorus and the associated density mode with the frequency equal to that of lower band chorus. In this letter, with a one-dimensional (1-D) particle-in-cell (PIC) simulation model, we have successfully reproduced multiband chorus waves. During the simulation, the significant density fluctuation is driven by the fluctuating electric field along the wave vector of the pump wave (lower band chorus), which can be directly observed in this self-consistent plasma system. Then, the second harmonic of the pump whistler-mode wave (upper band chorus) is generated. After quantitatively analyzing resonant conditions among wave numbers, we can confirm that the generation is caused due to the coupling between the pump wave and the density fluctuation along its wave vector. The third harmonic can also be excited through lower band cascade if the pump whistler-mode wave has a sufficiently large amplitude. Our simulation results not only provide a theoretical support to the mechanism of lower band cascade to generate multiband chorus but also propose a new pattern of evolution for whistler-mode waves in the Earth's magnetosphere.

1. Introduction

Whistler-mode chorus waves are important electromagnetic emissions in the Earth's magnetosphere, which have been commonly believed to account for both the source of relativistic (~ MeV) electrons in the Van Allen radiation belt [*Reeves et al.*, 2013; *Thorne et al.*, 2013; *Mourenas et al.*, 2014] and the precipitation of low-energy (~10 keV) electrons into the Earth's atmosphere [*Thorne et al.*, 2010; *Ni et al.*, 2011; *Nishimura et al.*, 2013]. Chorus waves are generated through the cyclotron resonance with injected plasma sheet electrons in the inner magnetosphere [*Li et al.*, 2010; *Gao et al.*, 2014b; *Fu et al.*, 2014], and their main source region is located near the magnetic equator [*LeDocq et al.*, 1998; *Santolik et al.*, 2005; *Li et al.*, 2009]. Chorus waves are usually detected in the frequency range of 0.1–0.8 f_{ce} (f_{ce} is the equatorial electron gyrofrequency), which typically exhibit three kinds of time-frequency spectrogram [*Li et al.*, 2011, 2012]: rising tone, falling tone, and hiss-like emission. What is very intriguing is that there is usually a power gap near 0.5 f_{ce}, separating chorus waves into two bands [*Tsurutani and Smith*, 1974; *Omura et al.*, 2009; *Li et al.*, 2012; *Fu et al.*, 2014]: lower band (0.1–0.5 f_{ce}) and upper band (0.5–0.8 f_{ce}).

Recently, based on the analysis of two chorus events observed by Time History of Events and Macroscale Interactions during Substorms (THEMIS) satellites in the Earth's radiation belt, *Gao et al.* [2016a] found that in two events the frequency of upper band chorus is about twice that of lower band chorus, and such a kind of chorus waves is called as multiband chorus waves. A generation mechanism for multiband chorus waves known as lower band cascade was also proposed, where upper band chorus is excited due to the wave-wave coupling between lower band chorus and the density fluctuation caused by the fluctuating electric field along the wave vector of lower band chorus. In this letter, with a one-dimensional (1-D) particle-in-cell (PIC) simulation model, we demonstrate that upper band chorus can be generated thorough lower band cascade and multiband chorus waves observed in the radiation belt can be explained by such mechanism. The amplitude ratios among harmonic waves and the pump wave are also investigated.

2. 1-D PIC Simulation Model and Initialization

A 1-D PIC simulation model with periodic boundary condition is employed to study lower band cascade, which only allows spatial variations in the x direction. The model retains full dynamics of electrons and

Table 1. Some Initial Parameters in the Simulation Model[a]

Parameter	Value	Parameter	Value
n_c/n_0	0.9	m_p/m_e	1836
v_{tc}/V_{Ae}	6×10^{-2}	ω_0/Ω_e	0.3
n_h/n_0	0.1	k_0V_{Ae}/Ω_e	0.86
v_{th}/V_{Ae}	0.4	θ	45^o
v_{tp}/V_{Ae}	1.4×10^{-3}	$\delta B_{yz}/B_0$	0.02

[a]These parameters include cold electron density n_c/n_0; cold electron thermal velocity v_{tc}/V_{Ae}; hot electron density n_h/n_0; hot electron thermal velocity v_{th}/V_{Ae}; proton thermal velocity v_{tp}/V_{Ae}; proton to electron mass ratio m_p/m_e; and wave frequency ω_0/Ω_e, wave number k_0V_{Ae}/Ω_e, wave normal angle θ, and magnetic amplitude $\delta B_{yz}/B_0$ of the pump wave.

protons by solving the relativistic motion equation of single-charged particle driven by the Lorentz force. The electric and magnetic fields are defined on grids and obtained by integrating the time-dependent Maxwell equations with a full explicit "Leapfrog" algorithm [*Birdsall and Langdon*, 1991]. The PIC simulation models have been widely employed in various research on space plasmas [*Fu et al*., 2006; *Lu et al*., 2010; *Du et al*., 2011]. It is reasonable to investigate the nonlinear evolution of whistler-mode waves with 1-D PIC model, since lower band cascade is a quasi-one-dimensional physical process along the wave vector of pump waves [*Gao et al*., 2016a]. The background magnetic field $\mathbf{B_0}$ is lying in the *x*-*z* plane, $\mathbf{B_0} = B_0(\cos\theta\hat{\mathbf{x}} + \sin\theta\hat{\mathbf{z}})$, where θ is the angle between the *x* axis and the background magnetic field. In the simulation model, the uniform and magnetized plasma consists of three components, cold electrons, cold protons, and hot electrons, which all satisfy the Maxwellian velocity distribution.

In this simulation, the units of space and time are the electron inertial length $\lambda_e = c/\omega_{pe}$ (c and ω_{pe} are the light speed and plasma frequency, respectively) and the inverse of electron gyrofrequency Ω_e^{-1}, respectively. The number of grid cells is $n_x = 2048$, and its size is set as $\Delta x = 0.036\lambda_e$, which means that there are 10 wave lengths in the simulation box. In order to reduce background noise to a very low level, we uniformly put on average 40,000 macroparticles in every cell for each species. The time step is $\Omega_e\Delta t = 0.005$. If we assume the background magnetic field to be $B_0 = 150$ nT at $L \approx 6$, and the plasma density to be $n_0 = 5\ \mathrm{cm}^{-3}$, which is a typical value in the Earth's magnetosphere [*Gao et al*., 2014c], then the light speed will be $c = 4.78V_{Ae}$ ($V_{Ae} = B_0/\sqrt{\mu_0 n_0 m_e}$ is the electron Alfven speed, where n_0 is the plasma density), or equivalently, the ratio of the electron plasma frequency ω_{pe} to gyrofrequency Ω_e is 4.78. Other important plasma and wave parameters in this simulation have been listed in Table 1. This initial setup has been obtained from the linear theory model based on the Vlasov-Maxwell equations described in Kennel's paper [1966]. It is worth noting that the system is initialized only with a pump monochromatic whistler-mode wave propagating along the *x* axis. The pump wave is set up by assigning fluctuating wave fields on each grid and fluctuating bulk velocity to each particle in the form of $A_i e^{i(k_0x+\phi_i)}$ (A_i and ϕ_i are the related parameter and its initial phase, respectively) along the *x* axis. It should be noted that the frequency chirping of chorus waves is related to the inhomogeneity of the background magnetic field [*Omura et al*., 2008; *Tao et al*., 2014], but a homogeneous magnetic field is used in our simulation. In this paper, we only focus on the generation of harmonic waves of a pump monochromatic whistler-mode wave through lower band cascade.

3. Simulation Results

Figure 1 exhibits the time evolution of whistler-mode waves, including (a) the *k*-*t* spectrogram of the transverse fluctuating magnetic field $\delta B_\perp$ with respect to the wave vector, (b) the ω-t spectrogram of $\delta B_\perp$, and (c) the dispersion relation of whistler-mode waves. Here the transverse fluctuating magnetic field is defined as $\delta B_\perp = \sqrt{\delta B_y^2 + \delta B_z^2}$. In all panels, the pump wave and its second harmonic are denoted by "PW" and "SH," respectively. Initially, a pump whistler-mode wave with a wave number $k_0V_{Ae}/\Omega_e \approx 0.86$ is set up in the system. Meanwhile, we can find that one whistler-mode wave with $k \approx 2k_0$ begins to grow and reaches its saturation stage at about $150\,\Omega_e^{-1}$ (Figure 1a). This multiband spectrum is quite similar to the multiband chorus event reported in the work by *Gao et al*. [2016a, Figure 1]. In Figure 1b, there are also two bands shown in the $\omega - t$ spectrogram, which are separated by $0.5\,\Omega_e$. Here in order to get a higher-frequency resolution, we conduct the sliding short-time Fourier analysis with a window size of $200\,\Omega_e^{-1}$, which thus results in the occurrence of upper band waves from the very beginning in Figure 1b. The dispersion relation shown in Figure 1c also confirms that the second harmonic of the pump whistler-mode wave is successfully reproduced in this simulation. Besides, the generated waves propagate in the same direction as the pump whistler-mode wave, which is also consistent with observations [*Gao et al*., 2016a].

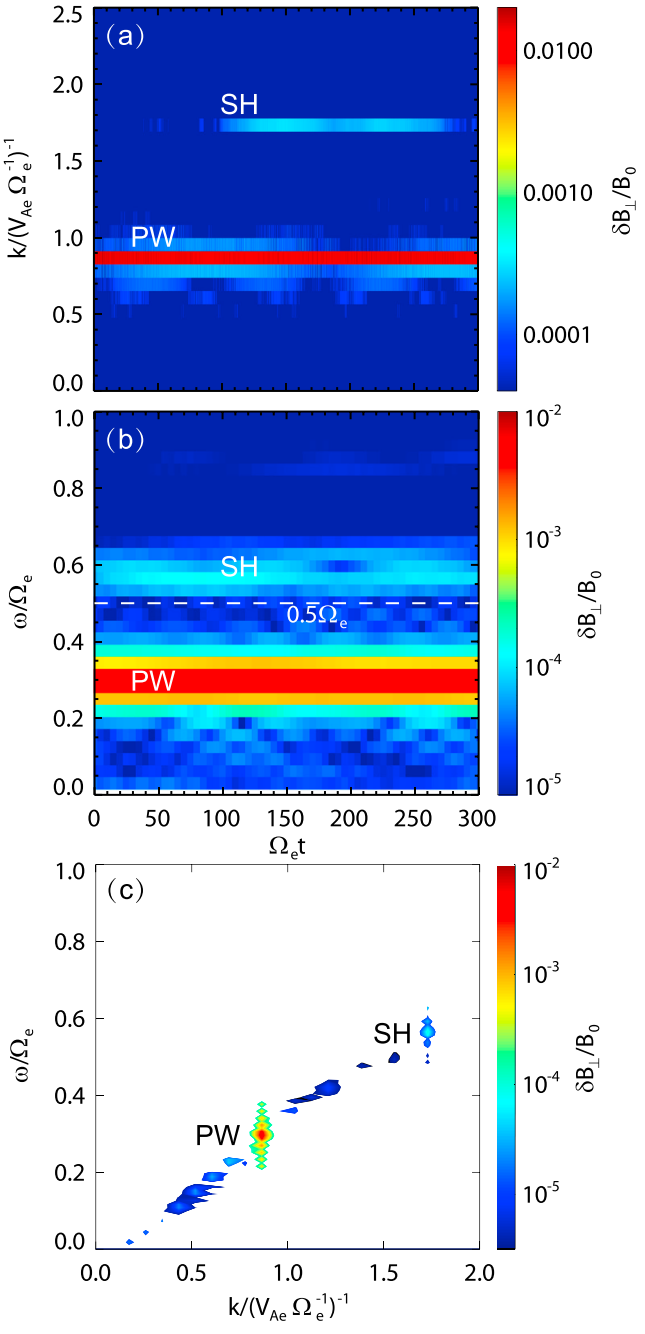

Figure 1. (a) The *k-t* spectrogram of perpendicular fluctuating magnetic fields ($\delta B_\perp/B_0$) obtained from the fast Fourier transform, (b) the $\omega - t$ spectrogram of $\delta B_\perp/B_0$ obtained by the short-time Fourier analysis, and (c) the dispersion relation of whistler-mode waves obtained from two-dimensional Fourier transform of $\delta B_\perp/B_0$. In all panels, the pump wave and its second harmonic are denoted by PW and SH, respectively. The 0.5 Ω_e is marked by the white dashed line in Figure 1b.

Figure 2 represents (a) the *k-t* spectrogram of the wave electric field δE_x along the wave vector, (b) the *k-t* spectrogram of the electron density fluctuation δn_e, and (c) the dispersion relation of δn_e. The distinct property of oblique whistler-mode waves is the existence of the fluctuating electric field along the wave vector of the pump wave, which can be clearly observed in Figure 2a. The density fluctuation along the wave vector of the pump wave is then driven quickly by the wave electric field, whose dominant wave number also turns up at about k_0 (Figure 2b). The density fluctuation shown here has been considered to play a key role in lower band cascade, but it cannot be directly measured by current satellites in the Earth's magnetosphere [*Gao et al.*, 2016a]. The dispersion relation of the density fluctuation displayed in Figure 2c further suggests that this density fluctuation should be caused by the pump whistler-mode wave, since it processes nearly the same wave number, frequency, and propagating direction as the pump wave.

The resonant conditions between different wave modes during the nonlinear evolution of the pump whistler-mode wave are also checked below. The bicoherence index is a powerful method to quantitatively measure the phase coupling among three wave modes, which has been commonly applied in many previous works [*van Milligen et al.*, 1995; *Nariyuki and Hada*, 2006; *Nariyuki et al.*, 2009; *Gao et al.*, 2014a; *Gao et al.*, 2016a]. In this letter, the bicoherence index *bc* is defined as

$$\left|\left\langle \delta n_e(k_{ne}) B_y(k_{By}) B_y^*(k_w)\right\rangle\right|^2 / \left\langle \left|\delta n_e(k_{ne}) B_y(k_{By})\right|^2\right\rangle \left\langle \left|B_y^*(k_w)\right|^2\right\rangle$$

(where $k_w = k_{ne} + k_{By}$, k_{ne}, and k_{By} are wave numbers of the fluctuating electron density and magnetic field and the bracket $\langle \cdots \rangle$ denotes an average over the $10\Omega_e^{-1}$ internal), and $\delta n_e(k_{ne})$ and $\delta B_y(k_{By})$ have been obtained through the Fourier analysis. The *bc* value ranges from 0 to 1, where an value of 1 means a strong resonance and a value of 0 means no resonant coupling. Figure 3a presents the bicoherence indices for $\Omega_e t = 110 - 120$. The time interval is chosen just after the second harmonic can be

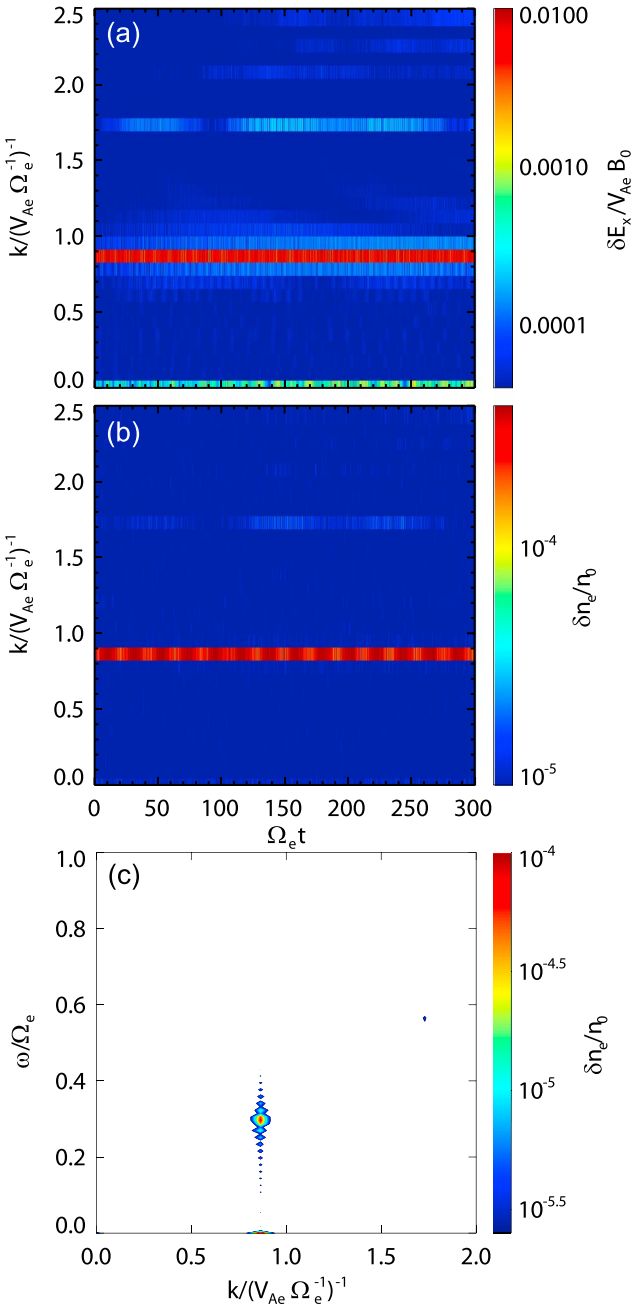

Figure 2. (a) The *k-t* spectrogram of wave electric fields $\delta E_x/B_0V_{Ae}$ along the wave vector, (b) the *k-t* spectrogram of electron density fluctuations $\delta n_e/n_0$, and (c) the dispersion relation of electron density fluctuations obtained from two-dimensional Fourier transform of $\delta n_e/n_0$.

clearly observed. In the panel, when the value of the bicoherence index is near 1, it means that there is a very strong resonance among k_{ne}, k_{By}, and k_w (i.e., $k_{ne}+k_{By}$). As shown in Figure 3a, there is a strong coupling among $k_{ne}V_{Ae}/\Omega_e \approx 0.86$, $k_{By}V_{Ae}/\Omega_e \approx 0.86$, and $k_wV_{Ae}/\Omega_e \approx 1.72$ during $\Omega_e t = 110-120$ with $bc \approx 0.6$. This convincingly demonstrates that the second harmonic of the pump whistler-mode wave is generated due to the coupling between the pump wave and the density fluctuation. The temporal profiles of the magnetic intensity $\delta B_\perp/B_0$ for the pump whistler-mode wave k_0 (solid black line) and its second harmonic 2 k_0 (dashed black line) have been illustrated in Figure 3b, respectively. Note that the amplitude of the second harmonic has been artificially amplified by 10 times for visualization purpose. Initially, there is only the pump wave with the amplitude $\delta B_\perp/B_0 \approx 0.02$ in the system. Then, the second harmonic of the pump wave starts to increase from the noise level, while the amplitude of the pump wave slowly decreases. It indicates that the energy of the pump whistler-mode wave is gradually transferred to the higher-frequency whistler-mode waves. The second harmonic reaches its maximum wave amplitude ($\delta B_\perp/B_0 \approx 0.00035$) at about $\Omega_e t = 150$, which is roughly one and half orders smaller than that of the pump whistler-mode wave.

We also perform another simulation run with $\omega_0/\Omega_e = 0.2$, $k_0V_{Ae}/\Omega_e = 0.63$, $\theta = 45^\circ$, and $\delta B_{yz}/B_0 = 5\,\%$, which is assumed at a large $L = 11$ with the background magnetic field $B_0 \approx 40$ nT and the plasma density $n_0 \approx 0.4cm^{-3}$. Figure 4 shows the time evolution of whistler-mode waves, including (a) the *k-t* spectrogram of the transverse fluctuating magnetic field $\delta B_\perp$ with respect to the wave vector, (b) the $\omega - t$ spectrogram of $\delta B_\perp$, and (c) the magnetic amplitudes $\delta B_\perp$ of the pump wave (PW), its second harmonic (SH), and its third harmonic (TH). What is most interesting is that after the second harmonic obtains a sufficiently large wave amplitude, the third harmonic also begins to grow at $\Omega_e t \approx 150$ (Figure 4a). As a result, there are three bands observed in either *k-t* (Figure 4a) or $\omega - t$ (Figure 4b) spectrogram, which is quite similar to the strong multiband chorus event reported by *Gao et al.* [2016a, Figure 5]. Besides, as shown in Figure 4c, the amplitude of the second harmonic is always 1–2 orders

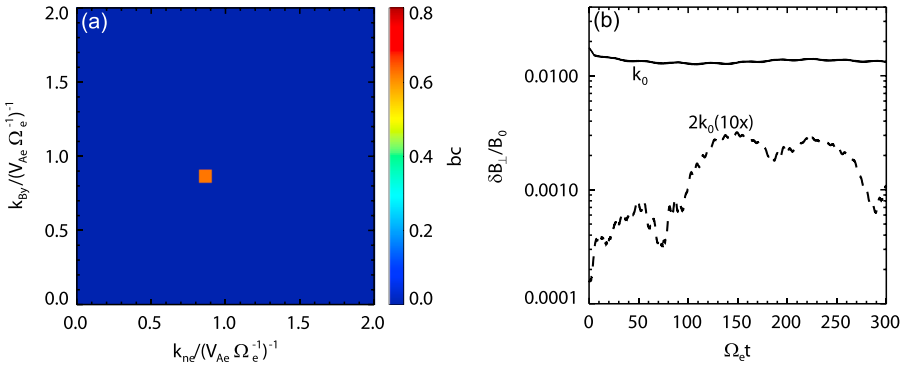

Figure 3. (a) The bicoherence indices among density fluctuations (k_{ne}) and whistler-mode waves (k_{By}) for $\Omega_e t = 110 - 120$ and (b) the temporal profiles of the magnetic intensity $\delta B_\perp/B_0$ for the pump whistler-mode wave k_0 (black solid line) and its second harmonic 2 k_0 (black dashed line). Here the amplitude of the second harmonic has been artificially amplified by 10 times for visual clarity.

smaller than that of the pump whistler wave, while the amplitude ratio between second and third harmonics can become within an order of magnitude during the simulation.

4. Conclusions and Discussion

In this letter, with a 1-D PIC simulation model, we have studied the nonlinear evolution of a nonparallel whistler-mode wave. The lower band cascade mechanism has been successfully verified. The significant density fluctuation involved in the lower band cascade is driven by the fluctuating electric field along the wave vector of the pump wave, which can be clearly observed in our simulation. Based on the analysis of resonant conditions among wave numbers, it is shown that the second harmonic of the pump whistler-mode wave is generated due to the coupling between the pump wave and the density fluctuation along its wave vector, while the third harmonic may also be excited through lower band cascade if the pump whistler-mode wave has a sufficiently large amplitude. Therefore, our simulation results verify that lower band cascade proposed in *Gao et al.* [2016a] provides a mechanism to generate multiband chorus.

In this simulation, the pump whistler-mode wave are cascaded not only to its second harmonic (Figure 1) but also to its third harmonic (Figure 4), and these waves have the same propagating direction. Note that the density fluctuation is caused by the fluctuating electric field along the wave vector, which is consistent with the compressibility of the oblique whistler-mode wave. The precise nonlinear mechanism leading to the observed lower band cascade and the generation of what looks like a second harmonic of the pump chorus wave still remains unclear at this stage. However, our simulation results agree well with recent observations in the magnetosphere. A full nonlinear theoretical analysis of present results is left for a future work. Our results are quite similar to the multiband chorus event reported by *Gao et al.* [2016a; Figures 1 and 5]. Besides, according to their observations, the amplitude of the second harmonic of the lower band chorus wave is observed to be 1–2 orders smaller than that of the lower band chorus wave, while the amplitude of the third harmonic is also 1–2 orders smaller than that of the second harmonic. As shown in Figures 3b and 4c, the amplitude ratio of the second harmonic to the pump wave in the simulation is quite consistent with the observation shown in *Gao et al.* [2016a]. However, the amplitude ratio of the third harmonic to the second harmonic is changing significantly with the time, from ~0.1 to ~0.4 (Figure 4). This may indicate that the third harmonic is not necessarily much weaker ($< 10^{-1}$) than the second harmonic for multiband chorus waves, but this is still needed to be verified in further observations.

The frequency chirping is an important characteristic of chorus waves, which is related to the inhomogeneity of the background magnetic field [*Omura et al.*, 2008; *Tao et al.*, 2014], and it cannot be studied with the simulation model in this letter. Here a homogeneous magnetic field is used in the simulation model, and we focus on the generation of harmonics of a pump monochromatic whistler-mode wave without frequency chirping. Our results provide a theoretic support for the generation of multiband chorus waves through lower band cascade and also imply that lower band cascade is a general nonlinear process for whistler-mode waves regardless of their time-frequency structures. Therefore, lower band cascade should be observed not only

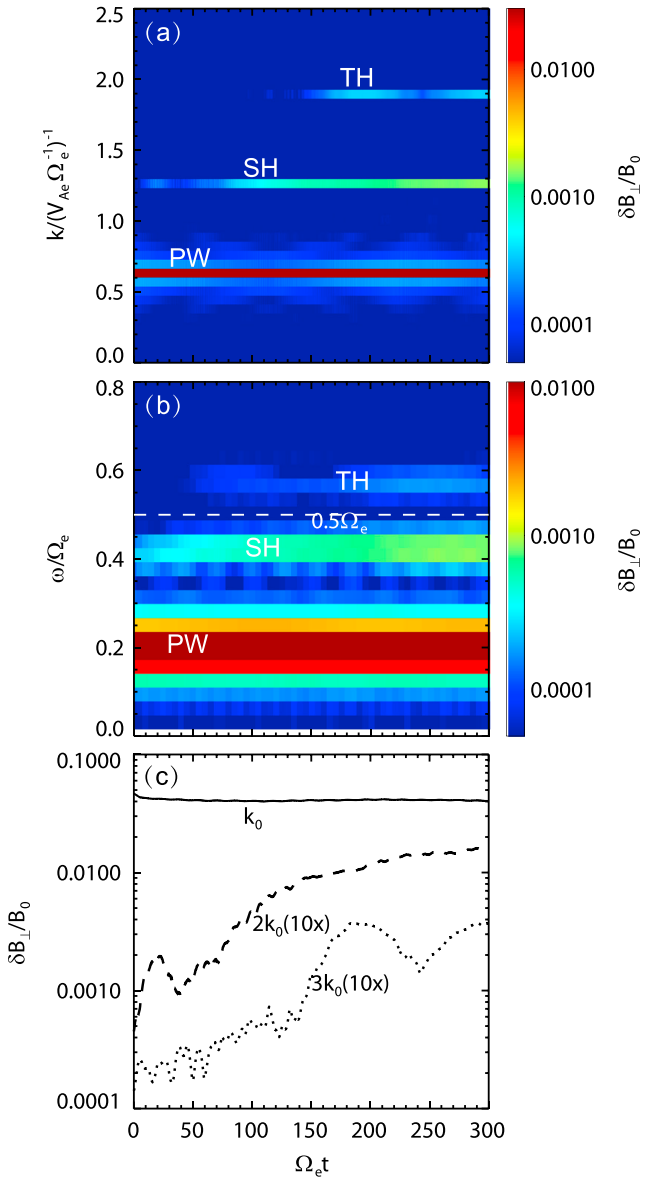

Figure 4. (a) The *k-t* spectrogram of perpendicular fluctuating magnetic fields ($\delta B_\perp/B_0$) obtained from the FFT, (b) the $\omega - t$ spectrogram of $\delta B_\perp/B_0$ obtained by the short-time Fourier analysis, and (c) the temporal profiles of the magnetic intensity $\delta B_\perp/B_0$ for the pump whistler-mode wave k_0 (black solid line), its second harmonic 2 k_0 (black dashed line), and its third harmonic 3 k_0. In all panels, the pump wave, its second harmonic, and its third harmonic are denoted by PW, SH, and TH, respectively. The 0.5 Ω_e is marked by the white dashed line in Figure 4b.

for the discrete chorus waves as reported in *Gao et al.* [2016a] but also for the hiss-like chorus waves in the Earth's magnetosphere. In this regime, as chorus waves propagate away from their source region (i.e., magnetic equator), their energy may be transported to higher-frequency channels via lower band cascade due to the increase of the wave normal angle, if the wave amplitude is still sufficiently large.

Recently, rising tones of lower band chorus have been thoroughly studied by means of theories [*Omura et al.*, 2008], simulations [*Omura et al.*, 2008; *Fu et al.*, 2014], and observations [*Santolik et al.*, 2003; *Li et al.*, 2011, 2012, 2013; *Gao et al.*, 2014b, 2016b], but the generation of upper band chorus, or equivalently the power gap between lower and upper bands at about 0.5 f_{ce}, still remains a mystery. Although some potential mechanisms have been proposed to explain the generation of upper band chorus waves and the formation of the power minimum at 0.5 f_{ce}, such as a strong damping at 0.5 f_{ce} [*Omura et al.*, 2009], different source regions [*Bell et al.*, 2009], and different free energy sources [*Fu et al.*, 2014], they are still under debate and lack direct observational evidences. Combined with the observational study by *Gao et al.* [2016a], our simulation results may provide an explanation for the generation of one kind of upper band chorus, whose amplitude is smaller than that of upper band chorus as reported in *Santolik et al.* [2003], and also propose a fresh view of the nonlinear evolution of whistler-mode waves in the Earth's magnetosphere.

Acknowledgments
This research was supported by the NSFC grants 41604128, 41631071, 41331067, 41421063; Key Research Program of Frontier Sciences, CAS (Chinese Academy of Sciences) QYZDJ-SSW-DQC010, and Youth Innovation Promotion Association of Chinese Academy of Sciences (2016395). The simulation data will be preserved on a long-term storage system and will be made available upon request to the corresponding author.

References

Bell, T. F., U. S. Inan, N. Haque, and J. S. Pickett (2009), Source regions of banded chorus, *Geophys. Res. Lett.*, *36*, L11101, doi:10.1029/2009GL037629.

Birdsall, C. K., and A. B. Langdon (1991), *Plasma Physics Via Computer Simulation*, IOP Publ, Philadelphia, Pa.

Du, A. M., M. Y. Wu, Q. M. Lu, C. Huang, and S. Wang (2011), Transverse instability and magnetic structures associated with electron phase space holes, *Phys. Plasmas*, *18*, 032104.

Fu, X., Q. M. Lu, and S. Wang (2006), The process of electron acceleration during collisionless magnetic reconnection, *Phys. Plasmas*, *13*, 012309.

Fu, X., et al. (2014), Whistler anisotropy instabilities as the source of banded chorus: Van Allen Probes observations and particle-in-cell simulations, *J. Geophys. Res. Space Physics*, *119*, 8288–8298, doi:10.1002/2014JA020364.

Gao, X. L., Q. M. Lu, X. Li, Y. F. Hao, X. Tao, and S. Wang (2014a), Ion dynamics during the parametric instabilities of a left-hand polarized Alfven wave in a proton-electron-alpha plasma, *Astrophys. J.*, *780*, 56, doi:10.1088/0004-637X/780/1/56.

Gao, X. L., W. Li, R. M. Thorne, J. Bortnik, V. Angelopoulos, Q. M. Lu, X. Tao, and S. Wang (2014b), New evidence for generation mechanisms of discrete and hiss-like whistler mode waves, *Geophys. Res. Lett.*, *41*, 4905–4811, doi:10.1002/2014GL060707.

Gao, X. L., W. Li, R. M. Thorne, J. Bortnik, V. Angelopoulos, Q. M. Lu, X. Tao, and S. Wang (2014c), Statistical results describing the bandwidth and coherence coefficient of whistler mode waves using THEMIS waveform data, *J. Geophys. Res. Space Physics*, *119*, 8992–9003, doi:10.1002/2014JA020158.

Gao, X. L., Q. M. Lu, J. Bortnik, W. Li, L. Chen, and S. Wang (2016a), Generation of multiband chorus by lower band cascade in the Earth's magnetosphere, *Geophys. Res. Lett.*, *43*, 2343–2350, doi:10.1002/2016GL068313.

Gao, X. L., D. Mourenas, W. Li, A. V. Artemyev, Q. M. Lu, X. Tao, and S. Wang (2016b), Observational evidence of generation mechanisms for very oblique lower band chorus using THEMIS waveform data, *J. Geophys. Res. Space Physics*, *121*, 6732–6748, doi:10.1002/2016JA022915.

Kennel, C. F., and F. Engelman (1966), Velocity space diffusion from weak plasma turbulence in a magnetic field, *Phys. Fluids*, *9*(12), 2377, doi:10.1063/1.1761629.

LeDocq, M. J., D. A. Guernett, and G. B. Hospodarsky (1998), Chorus source locations from VLF Poynting flux measurements with the Polar spacecraft, *Geophys. Res. Lett.*, *25*, 4063–4066, doi:10.1029/1998GL900071.

Li, W., R. M. Thorne, V. Angelopoulos, J. Bortnik, C. M. Cully, B. Ni, O. LeContel, A. Roux, U. Auster, and W. Magnes (2009), Global distribution of whistler mode chorus waves observed on the THEMIS spacecraft, *Geophys. Res. Lett.*, *36*, L09104, doi:10.1029/2009GL037595.

Li, W., R. M. Thorne, J. Bortnik, Y. Nishimura, V. Angelopoulos, L. Chen, J. P. McFadden, and J. W. Bonnell (2010), Global distributions of suprathermal electrons observed on THEMIS and potential mechanisms for access into the plasmasphere, *J. Geophys. Res.*, *115*, A00J10, doi:10.1029/2010JA015687.

Li, W., J. Bortnik, R. M. Thorne, and V. Angelopoulos (2011), Global distribution of wave amplitudes and wave normal angles of chorus waves using THEMIS wave observations, *J. Geophys. Res.*, *116*, A12205, doi:10.1029/2011JA017035.

Li, W., R. M. Thorne, J. Bortnik, X. Tao, and V. Angelopoulos (2012), Characteristics of hiss-like and discrete whistler-mode emissions, *Geophys. Res. Lett.*, *39*, L18106, doi:10.1029/2012GL053206.

Li, W., et al. (2013), Characteristic of the Poynting flux and wave normal vectors of whistler-mode waves observed on THEMIS, *J. Geophys. Res. Space Physics*, *118*, 1461–1471, doi:10.1002/jgra.50176.

Lu, Q. M., L. H. Zhou, and S. Wang (2010), Particle-in-cell simulations of whistler waves excited by an electron kappa distribution in space plasma, *J. Geophys. Res.*, *115*, A02213, doi:10.1029/2009JA014580.

Mourenas, D., A. Artemyev, O. Agapitov, and V. Krasnoselskikh (2014), Consequences of geomagnetic activity on energization and loss of radiation belt electrons by oblique chorus waves, *J. Geophys. Res. Space Physics*, *119*, 2775–2796, doi:10.1002/2013JA019674.

Nariyuki, Y., and T. Hada (2006), Remarks on nonlinear relation among phases and frequencies in modulational instabilities of parallel propagating Alfven waves, *Nonlinear Proc. Geophys.*, *13*, 425.

Nariyuki, Y., T. Hada, and K. Tsubouchi (2009), Parametric instabilities of circularly polarized Alfven waves in plasmas with beam protons, *J. Geophys. Res.*, *114*, A07102, doi:10.1029/2009JA014178.

Ni, B. B., R. M. Thorne, Y. Y. Shprits, K. G. Orlova, and N. P. Meredith (2011), Chorus-driven resonant scattering of diffuse auroral electrons in nondipolar magnetic fields, *J. Geophys. Res.*, *116*, A06225, doi:10.1029/2011JA016453.

Nishimura, Y., et al. (2013), Structures of dayside whistler-mode waves deduced from conjugate diffuse aurora, *J. Geophys. Res. Space Physics*, *118*, 664–673, doi:10.1029/2012JA018242.

Omura, Y., Y. Katoh, and D. Summers (2008), Theory and simulation of the generation of whistler-mode chorus, *J. Geophys. Res.*, *113*, A04223, doi:10.1029/2007JA012622.

Omura, Y., M. Hikishima, Y. Katoh, D. Summers, and S. Yagitani (2009), Nonlinear mechanisms of lower-band and upper-band VLF chorus emissions in the magnetosphere, *J. Geophys. Res.*, *114*, A07217, doi:10.1029/2009JA014206.

Reeves, G. D., et al. (2013), Electron acceleration in the heart of the Van Allen radiation belts, *Science*, *341*, 991–994.

Santolik, O., D. A. Gurnett, and J. S. Pickett (2003), Spatio-temporal structure of storm-time chorus, *J. Geophys. Res.*, *108*(A7), 1287, doi:10.1029/2002JA009791.

Santolik, O., D. A. Gurnett, J. S. Pickett, M. Parrot, and N. Cornilleau-Wehirlin (2005), Central position of the source region of storm-time chorus, *Planet. Space Sci.*, *53*, 299–305, doi:10.1016/j.pss.2004.09.056.

Tao, X., Q. Lu, S. Wang, and L. Dai (2014), Effects of magnetic field configuration on day-night asymmetry of chorus occurrence rate: A numerical study, *Geophys. Res. Lett.*, *41*, 6577–6582, doi:10.1002/2014GL061493.

Thorne, R. M., B. Ni, X. Tao, R. B. Horne, and N. P. Meredith (2010), Scattering by chorus waves as the dominant cause of diffuse auroral precipitation, *Nature*, *467*, 943.

Thorne, R. M., et al. (2013), Rapid local acceleration of relativistic radiation-belt electrons by magnetospheric chorus, *Nature*, *504*, 411.

Tsurutani, B. T., and E. J. Smith (1974), Postmidnight chorus: A substorm phenomenon, *J. Geophys. Res.*, *79*, 118–127, doi:10.1029/JA079i001p00118.

van Milligen, B. P., E. Sanchez, T. Estrada, C. Hidalgo, B. Branas, B. Carreras, and L. Garcia (1995), Wavelet bicoherence: A new turbulence analysis tool, *Phys. Plasmas*, *2*, 3017.